

WAVE-ATTENUATION-1D: AN IDEALIZED ONE-DIMENSIONAL  
FRAMEWORK FOR WAVE ATTENUATION THROUGH COASTAL  
VEGETATION USING NUMBA-ACCELERATED SHALLOW  
WATER EQUATIONS

SANDY H.S. HERHO<sup>1,2,3</sup>, IWAN P. ANWAR<sup>2,3</sup>, FARUQ KHADAMI<sup>2</sup>,  
THEO R.E.B.N. NDRURU<sup>2</sup>, RUSMAWAN SUWARMAN<sup>4</sup>,  
DASAPTA E. IRAWAN<sup>5\*</sup>

<sup>1</sup>*Department of Earth and Planetary Sciences, University of California,  
Riverside, 900 University Ave., Riverside, CA 92521, USA*

<sup>2</sup>*Applied and Environmental Oceanography Research Group,  
Bandung Institute of Technology (ITB), Jalan Ganesha 10, Bandung, 40132,  
West Java, Indonesia*

<sup>3</sup>*Samudera Sains Teknologi (SST) Ltd., Gang Sarimanah XIII/67, Bandung,  
40151, West Java, Indonesia*

<sup>4</sup>*Atmospheric Science Research Group, Bandung Institute of Technology  
(ITB), Jalan Ganesha 10, Bandung, 40132, West Java, Indonesia*

<sup>5</sup>*Applied Geology Research Group, Bandung Institute of Technology (ITB),  
Jalan Ganesha 10, Bandung, 40132, West Java, Indonesia*

[Received: 22 April 2025. Accepted: 6 March 2026]

doi: <https://doi.org/10.55787/jtams.2026.1.AI00236>

**ABSTRACT:** Coastal vegetation provides critical wave attenuation for shore-line protection, but existing models are computationally prohibitive or lack educational transparency. We present wave-attenuation-1d, an open-source Python package implementing linearized shallow water equations with vegetation-induced drag. The model uses fourth-order Runge-Kutta integration on a staggered grid, achieving unconditional stability through implicit treatment of the drag term. Numerical experiments with monochromatic waves through 40-meter vegetation patches demonstrate transmission coefficients from 0.655 (sparse) to 0.010 (dense vegetation), corresponding to 34.5% and 99.0% wave height reductions. While the one-dimensional framework simplifies three-dimensional flows and flexible vegetation dynamics, it provides a computationally efficient baseline for understanding wave-vegetation interactions. The package features standardized NetCDF output and modular architecture, bridging research-grade simulations and accessible educational tools for exploring nature-based coastal protection solutions.

**KEY WORDS:** coastal protection, coastal vegetation, nature-based solutions, numerical modeling, shallow water equations, wave attenuation.

---

\*Corresponding author e-mail: [dasaptaerwin@itb.ac.id](mailto:dasaptaerwin@itb.ac.id)

## NOTATIONS

$x, z$	[m]	Horizontal and vertical coordinates	$T = 2\pi/\omega$	[s]	Wave period
			$\lambda$	[m]	Wavelength
$t$	[s]	Time	$c_0 = \sqrt{gh}$	[m/s]	Shallow water wave celerity
$L$	[m]	Domain length	$x_{v,1}, x_{v,2}$	[m]	Vegetation zone boundaries
$h$	[m]	Still water depth	$\chi_{\text{veg}}(x)$		Vegetation indicator function
$\eta$	[m]	Free surface elevation	$C_D$		Bulk drag coefficient
$H = h + \eta$	[m]	Total water depth	$N$	[stems/m <sup>2</sup> ]	Stem density
$u, \bar{u}$	[m/s]	Horizontal velocity, depth-averaged	$d_s$	[m]	Stem diameter
			$h_v$	[m]	Vegetation height
$p$	[Pa]	Pressure	$u_0$	[m/s]	Characteristic velocity amplitude
$\rho$	[kg/m <sup>3</sup> ]	Fluid density	$c_D$	[s <sup>-1</sup> ]	Linearized drag coefficient
$g$	[m/s <sup>2</sup> ]	Gravitational acceleration	$K_t$		Wave transmission coefficient
$A$	[m]	Wave amplitude			
$\omega$	[rad/s]	Angular frequency			

## 1 INTRODUCTION

Coastal vegetation provides natural defense against wave attack, with field observations demonstrating substantial wave height reductions through marsh systems and significant attenuation through mangrove forests during tropical cyclones [1, 2]. The theoretical foundation for wave attenuation by vegetation traces to Dalrymple et al. [3], who adapted the Morison equation to model drag forces on rigid cylinders representing plant stems. Subsequent refinements incorporated probabilistic stem distributions [4] and extended the framework to random waves using spectral methods [5].

Laboratory experiments revealed limitations of the rigid-cylinder approximation. Bradley and Houser [6] demonstrated that plant flexibility substantially reduces drag coefficients, while three-dimensional flow structures generate momentum transport mechanisms absent from depth-averaged formulations [7]. Contemporary advances include flexible vegetation dynamics through fluid-structure interaction models [8, 9], extension to spectral wave environments [10–12], and integration into phase-resolving codes [13–16].

Despite these advances, a gap exists between sophisticated research models and practical tools accessible to coastal engineers. High-fidelity simulations remain computationally prohibitive, while commercial software implements vegetation effects through opaque parameterizations. Open science principles [17, 18] and Python’s scientific computing ecosystem [19–23] enable transparent, reproducible implementations. This work provides an open-source Python implementation accelerated through just-in-time compilation [24], achieving computational efficiency while maintaining code transparency for educational purposes.

## 2 METHODS

### 2.1 PROBLEM GEOMETRY AND GOVERNING EQUATIONS

We consider wave propagation through a one-dimensional coastal flume of length  $L$  containing a vegetation patch, as illustrated in Fig. 1. A Cartesian coordinate system is adopted with the horizontal  $x$ -axis oriented along the direction of wave propagation and the vertical  $z$ -axis pointing upward, with  $z = 0$  at the still water level. The domain extends from  $x = 0$  to  $x = L$ , with constant still water depth  $h$ . A vegetation patch occupies the region  $x_{v,1} \leq x \leq x_{v,2}$ , characterized by rigid cylindrical stems of diameter  $d_s$ , height  $h_v$ , and number density  $N$  (stems per unit horizontal area). The free surface elevation  $\eta(x, t)$  represents the vertical displacement from still water level, so that the total water depth is  $H(x, t) = h + \eta(x, t)$ .

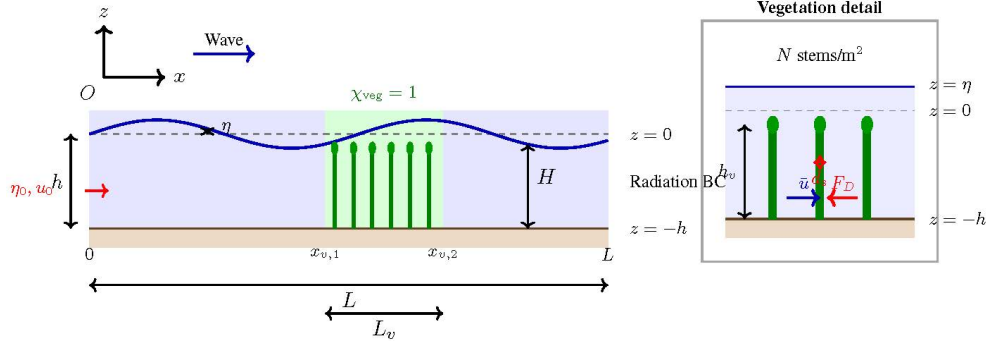


Fig. 1. Problem geometry and coordinate system. **Left:** Computational domain with vertical coordinate  $z$  measured from still water level ( $z = 0$ ). The bottom lies at  $z = -h$ , giving still water depth  $h$ . The free surface elevation  $\eta(x, t)$  is the displacement from  $z = 0$ , and total water depth is  $H = h + \eta$ . The vegetation zone extends from  $x_{v,1}$  to  $x_{v,2}$  where  $\chi_{veg} = 1$ . Waves enter from the left with prescribed  $\eta_0$  and  $u_0$ ; Sommerfeld radiation conditions apply at the right. **Right:** Vegetation detail showing rigid cylindrical stems with diameter  $d_s$ , height  $h_v$ , density  $N$ , depth-averaged velocity  $\bar{u}$ , and drag force  $F_D$  opposing the flow.

The motion of incompressible fluid is governed by the three-dimensional Navier-Stokes equations. Let  $\mathbf{u} = (u, v, w)^T$  denote the velocity vector with components in the  $x$ ,  $y$ , and  $z$  directions. The continuity equation expressing mass conservation is  $\nabla \cdot \mathbf{u} = 0$ , where  $\nabla = (\partial/\partial x, \partial/\partial y, \partial/\partial z)^T$  is the gradient operator. The momentum equation is

$$(1) \quad \rho \frac{D\mathbf{u}}{Dt} = -\nabla p + \mu \nabla^2 \mathbf{u} + \rho \mathbf{g} + \mathbf{F}_{\text{ext}},$$

where  $\rho$  is fluid density [ $\text{kg/m}^3$ ],  $p$  is pressure [Pa],  $\mu$  is dynamic viscosity [Pa·s],  $\mathbf{g} = (0, 0, -g)^T$  is gravitational acceleration with  $g = 9.81 \text{ m/s}^2$ ,  $\mathbf{F}_{\text{ext}}$  represents

external body forces  $[\text{N}/\text{m}^3]$ , and the material derivative  $D/Dt = \partial/\partial t + \mathbf{u} \cdot \nabla$  represents the rate of change following a fluid particle.

For shallow water flows where the horizontal length scale greatly exceeds the depth (aspect ratio  $\epsilon = h/L \ll 1$ ), vertical accelerations become negligible and the vertical momentum equation reduces to hydrostatic balance:  $\partial p/\partial z = -\rho g$ . Integration from depth  $z$  to the free surface, where pressure equals atmospheric pressure  $p_a$ , yields  $p = p_a + \rho g(\eta - z)$ . Depth integration of the horizontal momentum equations, using kinematic boundary conditions at the free surface and bottom, produces the shallow water equations. Defining the depth-averaged horizontal velocity as

$$(2) \quad \bar{u}(x, t) = \frac{1}{H} \int_{-h}^{\eta} u(x, z, t) dz,$$

and considering one-dimensional propagation along the  $x$ -axis, the depth-integrated continuity equation becomes  $\partial H/\partial t + \partial(H\bar{u})/\partial x = 0$ , and the momentum equation becomes  $\partial(H\bar{u})/\partial t + \partial(H\bar{u}^2)/\partial x + gH\partial\eta/\partial x = \bar{F}_x$ , where  $\bar{F}_x$  represents depth-integrated external forces per unit mass.

For small-amplitude waves satisfying  $|\eta| \ll h$ , we linearize by writing  $\eta = \varepsilon\eta'$  and  $u = \varepsilon u'$  where  $\varepsilon \ll 1$ , retaining only first-order terms, and dropping primes. The linearized shallow water equations become

$$(3) \quad \frac{\partial \eta}{\partial t} + h \frac{\partial u}{\partial x} = 0,$$

$$(4) \quad \frac{\partial u}{\partial t} + g \frac{\partial \eta}{\partial x} = -c_D \chi_{\text{veg}}(x)u,$$

where  $u(x, t)$  now denotes depth-averaged horizontal velocity, and the right-hand side of Eq. (4) represents linearized vegetation drag. The indicator function  $\chi_{\text{veg}}(x) = 1$  for  $x_{v,1} \leq x \leq x_{v,2}$  and zero elsewhere.

## 2.2 VEGETATION DRAG FORMULATION

The drag force on flow through an array of rigid cylinders follows from the Morison equation framework [3]. The time-averaged drag force per unit volume is  $\mathbf{F}_D = -\frac{1}{2}\rho C_D N d_s |\mathbf{u}| \mathbf{u}$ , where  $C_D$  is the bulk drag coefficient (dimensionless),  $N$  is stem density [stems/ $\text{m}^2$ ], and  $d_s$  is stem diameter [m]. The quadratic velocity dependence introduces nonlinearity that we remove through linearization.

For sinusoidal velocity  $u(t) = u_0 \sin(\omega t)$  with amplitude  $u_0$  and angular frequency  $\omega$ , we seek a linear drag coefficient  $c_D$  [ $\text{s}^{-1}$ ] such that the linearized force  $F_D^{\text{lin}} = -\rho c_D u$  dissipates the same energy per wave period as the quadratic drag. Following the Lorentz linearization procedure [28], the period-averaged dissipation

for quadratic drag is  $\langle P_{\text{quad}} \rangle = (4/3\pi) \cdot \frac{1}{2} \rho C_D N d_s u_0^3$ , while for linear drag it is  $\langle P_{\text{lin}} \rangle = \frac{1}{2} \rho c_D u_0^2$ . Equating these expressions yields

$$(5) \quad c_D = \frac{4}{3\pi} C_D N d_s u_0.$$

For vegetation of height  $h_v$  in water of depth  $h$ , accounting for partial submergence when  $h_v < h$ , the depth-averaged linearized drag coefficient becomes

$$(6) \quad c_D = \frac{4}{3\pi h} C_D N d_s h_v u_0.$$

The characteristic velocity  $u_0$  can be estimated from linear wave theory. For shallow water waves, the velocity amplitude relates to surface elevation amplitude  $A$  by  $u_0 = A\sqrt{g/h} = Ac_0/h$ , where  $c_0 = \sqrt{gh}$  is the shallow water wave celerity. Alternatively,  $u_0$  may be specified from field measurements or expected wave conditions [28, 29].

### 2.3 NUMERICAL IMPLEMENTATION

We employ a staggered grid arrangement to ensure proper coupling between surface elevation and velocity and to avoid spurious oscillations [25]. The domain  $[0, L]$  is divided into  $n_x$  cells of uniform width  $\Delta x$ . Surface elevation  $\eta$  is defined at cell centers  $x_i = (i - 1/2)\Delta x$  for  $i = 1, \dots, n_x$ , while velocity  $u$  is defined at cell faces  $x_{i+1/2} = i\Delta x$  for  $i = 0, \dots, n_x$ . The semi-discrete equations become

$$(7) \quad \frac{d\eta_i}{dt} = -\frac{h}{\Delta x} (u_{i+1/2} - u_{i-1/2}),$$

$$(8) \quad \frac{du_{i+1/2}}{dt} = -\frac{g}{\Delta x} (\eta_{i+1} - \eta_i) - c_D \chi_{i+1/2} u_{i+1/2},$$

where  $\chi_{i+1/2} = \chi_{\text{veg}}(x_{i+1/2})$ .

Time integration uses the classical fourth-order Runge-Kutta (RK4) method. Writing the system as  $d\mathbf{y}/dt = \mathbf{f}(\mathbf{y}, t)$  where  $\mathbf{y}$  contains all  $\eta_i$  and  $u_{i+1/2}$  values, the RK4 update from time level  $n$  to  $n + 1$  computes four intermediate stages:

$$(9) \quad \mathbf{k}_1 = \mathbf{f}(\mathbf{y}^n, t^n), \quad \mathbf{k}_2 = \mathbf{f}\left(\mathbf{y}^n + \frac{\Delta t}{2}\mathbf{k}_1, t^n + \frac{\Delta t}{2}\right),$$

$$(10) \quad \mathbf{k}_3 = \mathbf{f}\left(\mathbf{y}^n + \frac{\Delta t}{2}\mathbf{k}_2, t^n + \frac{\Delta t}{2}\right), \quad \mathbf{k}_4 = \mathbf{f}(\mathbf{y}^n + \Delta t\mathbf{k}_3, t^n + \Delta t),$$

and combines them as  $\mathbf{y}^{n+1} = \mathbf{y}^n + (\Delta t/6)(\mathbf{k}_1 + 2\mathbf{k}_2 + 2\mathbf{k}_3 + \mathbf{k}_4)$ .

The drag term  $-c_D\chi_{\text{veg}}u$  can become stiff for large  $c_D$ , potentially requiring impractically small time steps. We treat this term implicitly within each RK4 stage. For the isolated drag equation  $du^*/d\tau = F - c_D\chi u^*$ , where  $F$  is the pressure gradient contribution and  $\tau$  is sub-step time, the analytical solution is

$$(11) \quad u^*(\tau) = u^*(0)e^{-c_D\chi\tau} + \frac{F}{c_D\chi} (1 - e^{-c_D\chi\tau}).$$

This implicit treatment ensures unconditional stability for the drag term regardless of  $c_D\Delta t$ . The time step is constrained only by the CFL condition for advection:  $\Delta t \leq \text{CFL} \cdot \Delta x/c_0$ , where we use  $\text{CFL} = 0.4$ .

At the left boundary ( $x = 0$ ), we impose an incident sinusoidal wave:  $\eta(0, t) = A \sin(\omega t)$  and  $u(0, t) = (c_0/h)A \sin(\omega t)$ , with velocity determined from the linear shallow water relation for a progressive wave. At the right boundary ( $x = L$ ), we apply the Sommerfeld radiation condition  $\partial\eta/\partial t + c_0\partial\eta/\partial x = 0$ , discretized as  $\eta_{n_x}^{n+1} = \eta_{n_x}^n - c_0(\Delta t/\Delta x)(\eta_{n_x}^n - \eta_{n_x-1}^n)$ , allowing waves to exit without reflection.

The transmission coefficient  $K_t = H_{\text{out}}/H_{\text{in}}$  quantifies wave height reduction, computed from wave heights  $H = 2\sqrt{2}\sigma_\eta$  (where  $\sigma_\eta$  is the standard deviation of surface elevation) measured two wavelengths upstream and downstream of the vegetation zone, using the last 20% of simulation data to ensure quasi-steady conditions.

The solver is implemented in Python using NumPy [19] for array operations, with performance-critical loops accelerated via Numba [26] just-in-time compilation, achieving approximately  $100\times$  speedup. Output is stored in NetCDF-4 format [27] with CF-1.8 conventions.

## 2.4 NUMERICAL EXPERIMENTS

We simulate wave propagation through a 200 m flume with depth  $h = 2$  m. Monochromatic waves with amplitude  $A = 0.3$  m and period  $T = 10$  s ( $\omega = 0.628$  rad/s) enter from the left boundary. The wavelength is  $\lambda = c_0T = \sqrt{gh} \cdot T \approx 44.3$  m. Vegetation occupies  $x_{v,1} = 80$  m to  $x_{v,2} = 120$  m, giving patch length  $L_v = 40$  m. Two vegetation densities are considered: sparse ( $c_D = 0.14$  s $^{-1}$ , representative of *Spartina* salt marsh [28]) and dense ( $c_D = 1.4$  s $^{-1}$ , representative of mangrove forests [29]). Spatial resolution is  $\Delta x = 0.5$  m (89 points per wavelength), and simulations run for 50 wave periods.

## 3 RESULTS

Figure 2 presents the spatiotemporal evolution of wave energy density  $E = \frac{1}{2}\rho g\eta^2 + \frac{1}{2}\rho hu^2$ , representing potential plus kinetic energy per unit area. Dense vegetation (Fig. 2a) exhibits rapid attenuation, with energy decreasing from approximately 900 J/m $^3$

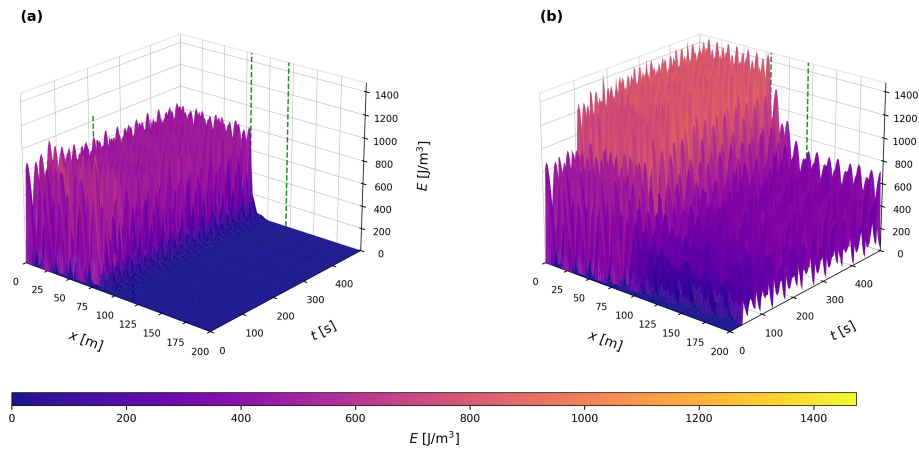


Fig. 2. Spatiotemporal evolution of wave energy density  $E$  [ $\text{J}/\text{m}^3$ ] for (a) dense vegetation ( $c_D = 1.4 \text{ s}^{-1}$ ) and (b) sparse vegetation ( $c_D = 0.14 \text{ s}^{-1}$ ). Dashed lines mark the vegetation zone ( $x = 80\text{--}120 \text{ m}$ ).

upstream to near-zero downstream. Sparse vegetation (Fig. 2b) produces gradual attenuation, maintaining  $400\text{--}600 \text{ J}/\text{m}^3$  downstream.

Figure 3 shows free surface elevation dynamics. Dense vegetation (Fig. 3a) reduces amplitudes from  $\pm 0.3 \text{ m}$  to less than  $\pm 0.01 \text{ m}$ . Sparse vegetation (Fig. 3b) preserves wave structure with reduced amplitude and visible partial reflection (up-

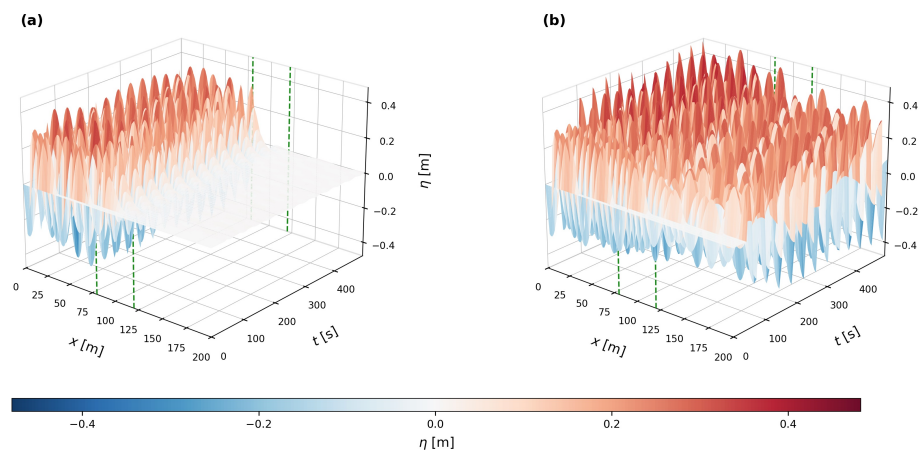


Fig. 3. Spatiotemporal evolution of free surface elevation  $\eta$  [m] for (a) dense and (b) sparse vegetation.

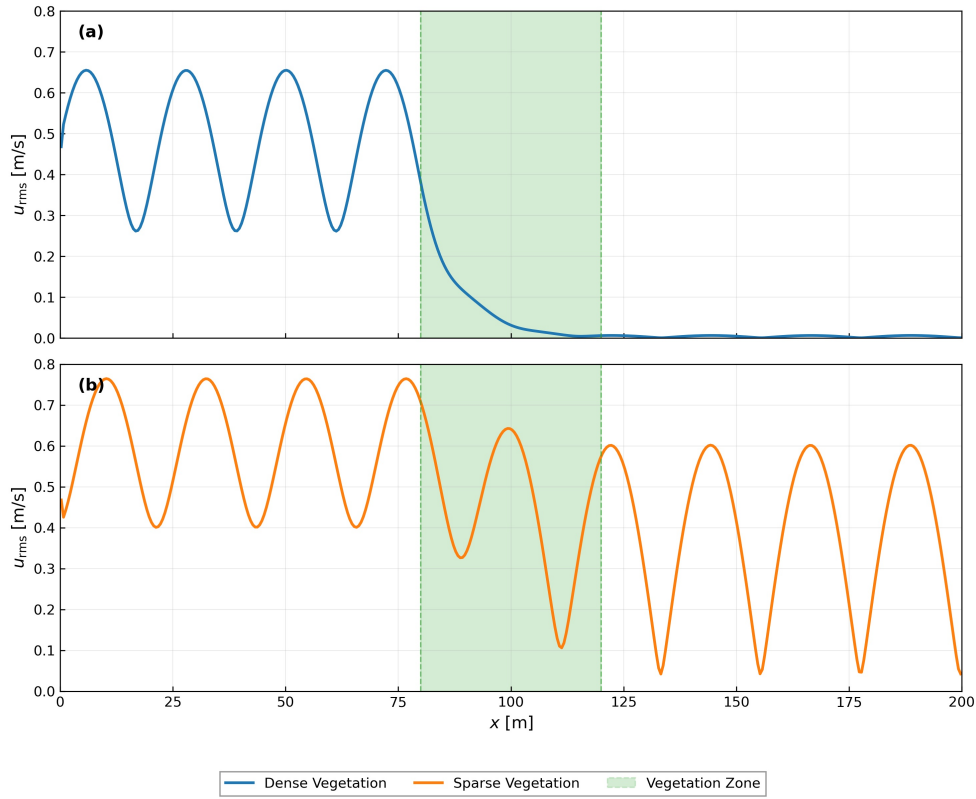


Fig. 4. Root-mean-square velocity  $u_{\text{rms}}$  [m/s] for (a) dense and (b) sparse vegetation. Shaded region indicates the vegetation zone.

stream amplitude modulation).

Figure 4 displays root-mean-square velocity  $u_{\text{rms}}(x) = \sqrt{\langle u^2 \rangle_t}$ , where  $\langle \cdot \rangle_t$  denotes time averaging over the last five periods. Dense vegetation (Fig. 4a) reduces  $u_{\text{rms}}$  from 0.655 m/s to 0.0005 m/s (99.2% reduction). Sparse vegetation (Fig. 4b) shows reduction from 0.765 m/s to 0.042 m/s (35.5% reduction).

Figure 5 shows the wave envelope  $A_{\text{env}}(x) = \max_t |\eta(x, t)|$ . Dense vegetation (Fig. 5a) produces exponential decay from 0.37 m upstream to 0.0006 m downstream. Sparse vegetation (Fig. 5b) shows oscillatory behavior due to partial reflection, with envelope ranging from 0.48 m to 0.025 m.

Table 1 summarizes quantitative results. The transmission coefficient is  $K_t = 0.655$  for sparse vegetation (34.5% height reduction) and  $K_t = 0.010$  for dense vegetation (99.0% reduction). Energy dissipation is 50.7% and 100.0%, respectively.

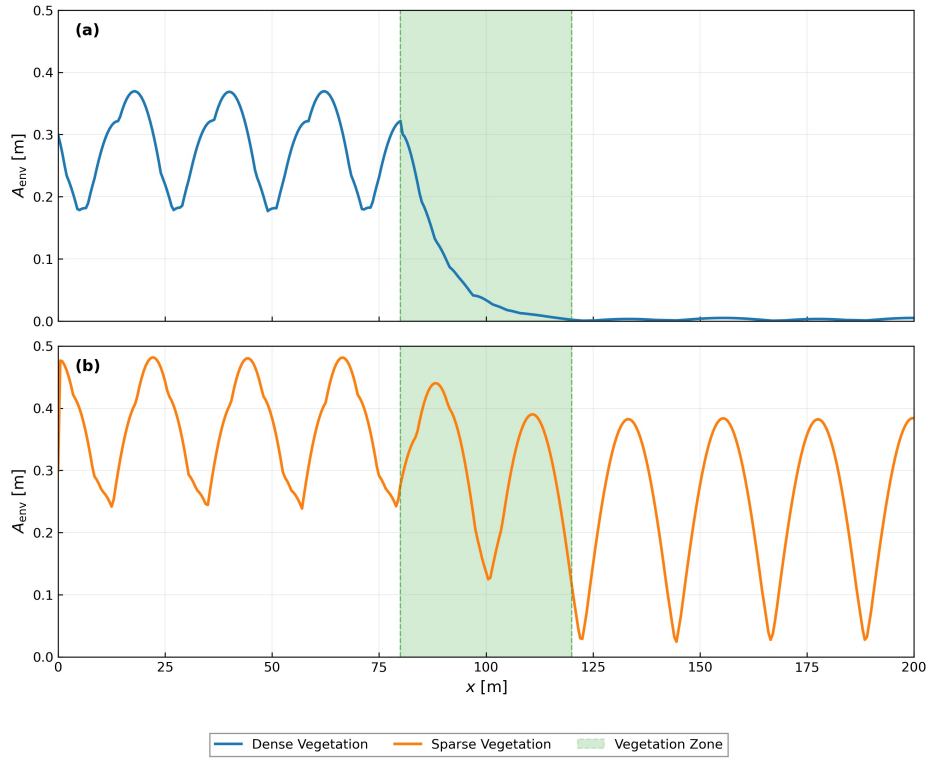


Fig. 5. Wave envelope  $A_{env}$  [m] for (a) dense and (b) sparse vegetation. Shaded region indicates the vegetation zone.

Table 1. Summary of wave attenuation results

Parameter	Sparse	Dense	Units
Drag coefficient ( $c_D$ )	0.14	1.4	$s^{-1}$
Mean amplitude before vegetation	0.369	0.276	m
Mean amplitude after vegetation	0.242	0.003	m
Amplitude reduction	34.5	99.0	%
Transmission coefficient ( $K_t$ )	0.655	0.010	–
Peak energy density	1479.0	910.9	$J/m^3$
Energy dissipation	50.7	100.0	%
Max $u_{rms}$ (upstream)	0.765	0.655	m/s
Min $u_{rms}$ (downstream)	0.042	0.0005	m/s
Velocity reduction	35.5	99.2	%

#### 4 DISCUSSION

The computed transmission coefficients are consistent with literature values for wave-vegetation interactions [31–33]. The sparse vegetation result ( $K_t = 0.655$ ) falls within typical experimental ranges for salt marsh under moderate waves. The dense vegetation result ( $K_t = 0.010$ ) represents extreme attenuation characteristic of thick mangrove forests, though such complete dissipation is rarely observed in field settings where nonlinear effects and three-dimensional flow structures reduce efficiency.

The linearized framework follows Dalrymple et al. [3] and Méndez and Losada [28], capturing fundamental physics while accepting simplifications. Rigid vegetation overestimates drag compared to flexible plants that reconfigure under flow [34]. Two-dimensional nonlinear formulations [36] capture spatial variations absent here but at greater computational cost. Combined vegetation-structure systems [37] exhibit interactions not representable by vegetation-only models.

Wave height decay through vegetation follows  $H(x) = H_0 \exp(-k_i x)$  where  $k_i = c_D/(2c_0)$  [28], assuming quasi-steady conditions and negligible reflection. The partial reflection visible for sparse vegetation (Fig. 5b) arises from impedance mismatch at vegetation boundaries. Extreme attenuation for dense vegetation may overestimate field performance because nonlinear effects including wave breaking become important for large  $c_D L_v/c_0$  [38, 39], the one-dimensional formulation cannot capture lateral flow diversion [40, 41], and real vegetation exhibits spatial heterogeneity not represented by uniform  $c_D$ .

The Numba-accelerated implementation achieves efficiency comparable to compiled languages while maintaining Python accessibility. The staggered grid ensures proper pressure-velocity coupling [25], and implicit drag treatment provides unconditional stability. Future work should address flexible vegetation [30], irregular wave spectra [10], and wave-current interactions [35].

#### 5 CONCLUSIONS

This study presents an efficient numerical framework for wave attenuation through coastal vegetation using linearized shallow water equations with vegetation drag. The formulation derives systematically from three-dimensional Navier-Stokes equations through depth integration and linearization, with explicit definitions of all variables and parameters. The numerical implementation employs a staggered grid with fourth-order Runge-Kutta integration and implicit drag treatment.

Numerical experiments yield transmission coefficients from 0.655 (sparse) to 0.010 (dense vegetation), corresponding to 34.5% and 99.0% wave height reductions, consistent with published observations. While the one-dimensional linear framework cannot capture full three-dimensional complexity, it provides a computationally ef-

efficient tool for preliminary assessment and education. The open-source Python implementation, available through PyPI, enables the coastal engineering community to apply and extend the framework.

#### ACKNOWLEDGEMENTS

Financial support for this work was provided by the Dean's Distinguished Fellowship (UCR, 2023) and the FITB-PPMI Program through grants FITB.PPMI-1-31-2025, and FITB.PPMI-1-8-2026.

#### AUTHOR CONTRIBUTIONS

**SHSH**: Conceptualization, Software, Writing-original. **IPA, FK**: Methodology, Supervision, Writing-review. **TREBNN**: Software, Writing-review. **RS, DEI**: Supervision, Writing-review.

#### OPEN RESEARCH

Software available via PyPI (<https://pypi.org/project/wave-attenuation-1d/>). Data and scripts at [https://github.com/sandyherho/suppl\\_wave\\_attenuation\\_1d](https://github.com/sandyherho/suppl_wave_attenuation_1d).

#### REFERENCES

- [1] I. MÖLLER, M. KUDELLA, F. RUPPRECHT, T. SPENCER, M. PAUL, B.K. VAN WESENBECK, G. WOLTERS, K. JENSEN, T. J. BOUMA, M. MIRANDA-LANGE, S. SCHIMMELS (2014) Wave Attenuation over Coastal Salt Marshes under Storm Surge Conditions. *Nature Geoscience* **7** 727-731.
- [2] A.L. MCIVOR, I. MÖLLER, T. SPENCER, M. SPALDING (2012) Storm Surge Reduction by Mangroves. *Natural Coastal Protection Series: Report 2* 1-35 .
- [3] R.A. DALRYMPLE, J.T. KIRBY, P.A. HWANG (1984) Wave Diffraction Due to Areas of Energy Dissipation. *Journal of Waterway, Port, Coastal, and Ocean Engineering* **110**(1) 67-79.
- [4] N. KOBAYASHI, A.W. RAICHLE, T. ASANO (1993) Wave Attenuation by Vegetation. *Journal of Waterway, Port, Coastal, and Ocean Engineering* **119**(1) 30-48.
- [5] F.J. MÉNDEZ, I.J. LOSADA, M.A. LOSADA (1999) Hydrodynamics Induced by Wind Waves in a Vegetation Field. *Journal of Geophysical Research: Oceans* **104** C8 18383-18396.
- [6] K. BRADLEY, C. HOUSER (2009) Relative Velocity of Seagrass Blades: Implications for Wave Attenuation in Low-Energy Environments. *Journal of Geophysical Research: Earth Surface* **114** F1.
- [7] H.M. NEPF (2012) Flow and Transport in Regions with Aquatic Vegetation. *Annual Review of Fluid Mechanics* **44** 123-142.
- [8] M. LUHAR, H.M. NEPF (2011) Flow-Induced Reconfiguration of Buoyant and Flexible Aquatic Vegetation. *Limnology and Oceanography* **56**(6) 2003-2017.

- [9] R.B. ZELLER, J.S. WEITZMAN, M.E. ABBETT, F.J. ZARAMA, O.B. FRINGER, J.R. KOSEFF (2014) Improved Parameterization of Seagrass Blade Dynamics and Wave Attenuation Based on Numerical and Laboratory Experiments. *Limnology and Oceanography* **59**(1) 251-266.
- [10] M.E. ANDERSON, J.M. SMITH (2014) Wave Attenuation by Flexible, Idealized Salt Marsh Vegetation. *Coastal Engineering* **83** 82-92.
- [11] R.S. JADHAV, Q. CHEN, J.M. SMITH (2013) Spectral Distribution of Wave Energy Dissipation by Salt Marsh Vegetation. *Coastal Engineering* **77** 99-107.
- [12] R.J. LOWE, J.L. FALTER, J.R. KOSEFF, S.G. MONISMITH, M.J. ATKINSON (2007) Spectral Wave Flow Attenuation within Submerged Canopies: Implications for Wave Energy Dissipation. *Journal of Geophysical Research: Oceans* **112** C5.
- [13] M. ZIJLEMA, G. STELLING, P. SMIT (2011) SWASH: An Operational Public Domain Code for Simulating Wave Fields and Rapidly Varied Flows in Coastal Waters. *Coastal Engineering* **58** 10 992-1012.
- [14] J.T. KIRBY (2003) Chapter 1 Boussinesq Models and Applications to Nearshore Wave Propagation, Surf Zone Processes and Wave-Induced Currents. In: V.C. Lakhan (ed) "Advances in Coastal Modeling". *Elsevier Oceanography Series* vol. **67**, Elsevier, pp. 1-41.
- [15] A. VAN ROOIJEN, R. LOWE, M. GHISALBERTI, R. MCCALL, J. HANSEN (2022) Modelling Wave Attenuation through Submerged Vegetation Canopies Using a Subgrid Canopy Flow Model. *Coastal Engineering* **176** 104153.
- [16] A.-E. PAQUIER, T. OUDART, C. LE BOUTEILLER, S. MEULÉ, P. LARROUDÉ, R.A. DALRYMPLE (2021) 3D Numerical Simulation of Seagrass Movement under Waves and Currents with GPUSPH. *International Journal of Sediment Research* **36**(6) 711-722.
- [17] R. RAMACHANDRAN, K. BUGBEE, K. MURPHY (2021) From Open Data to Open Science. *Earth and Space Science* **8**(5) e2020EA001562.
- [18] D.E. IRAWAN, O. POURRET, L. BESANÇON, S.H.S. HERHO, I.A. RIDLO, J. ABRAHAM (2024) Post-Publication Review: The Role of Science News Outlets and Social Media. *Annals of Library and Information Studies* **71**(4) 465-474.
- [19] C. HARRIS, K. MILLMAN, S. VAN DER WALT, R. GOMMERS, P. VIRTANEN, D. COURNAPEAU, E. WIESER, J. TAYLOR, S. BERG, N. SMITH, ET AL. (2020) Array Programming with NumPy. *Nature* **585** 357-362.
- [20] P. VIRTANEN, R. GOMMERS, T.E. OLIPHANT, M. HABERLAND, T. REDDY, D. COURNAPEAU, E. BUROVSKI, P. PETERSON, W. WECKESSER, J. BRIGHT, ET AL. (2020) SciPy 1.0: Fundamental Algorithms for Scientific Computing in Python. *Nature Methods* **17**(3) 261-272.
- [21] S. HERHO, I. ANWAR, K. HERHO, C. DHARMA, D. IRAWAN (2024) Comparing Scientific Computing Environments for Simulating 2D Non-Buoyant Fluid Parcel Trajectory under Inertial Oscillation: A Preliminary Educational Study. *Indonesian Physical Review* **7**(3) 451-468.
- [22] S.H.S. HERHO (2017) "Tutorial Pemrograman Python 2 Untuk Pemula". WCPL ITB, Bandung, Indonesia; <https://doi.org/10.31227/osf.io/bau26>.

- [23] S.H.S. HERHO, M.R. SYAHPUTRA, N.J. TRILAKSONO (2024) “Pengantar Metode Numerik Terapan: Menggunakan Python”. WCPL ITB, Bandung, Indonesia; <https://doi.org/10.22541/au.170689157.78106030/v1>.
- [24] S.H.S. HERHO, S.N. KABAN, D.E. IRAWAN, R. KAPID (2024) Efficient 1D Heat Equation Solver: Leveraging Numba in Python. *Eksakta: Berkala Ilmiah Bidang MIPA* 25(2) 126-137.
- [25] R.J. LEVEQUE (2002) “Finite Volume Methods for Hyperbolic Problems”. Cambridge University Press, Cambridge, UK; <https://doi.org/10.1017/CBO9780511791253>.
- [26] S.K. LAM, A. PITROU, S. SEIBERT (2015) Numba: A LLVM-Based Python JIT Compiler. In: *Proceedings of the Second Workshop on the LLVM Compiler Infrastructure in HPC*, pp. 1-6.
- [27] R.K. REW, G.P. DAVIS (1990) NetCDF: An Interface for Scientific Data Access. *IEEE Computer Graphics and Applications* 10(4) 76-82.
- [28] F.J. MÉNDEZ, I.J. LOSADA (2004) An Empirical Model to Estimate the Propagation of Random Breaking and Nonbreaking Waves over Vegetation Fields. *Coastal Engineering* 51(2) 103-118.
- [29] Y. MAZDA, M. MAGI, M. KOGO, P.N. HONG (1997) Mangroves as a Coastal Protection from Waves in the Tong King Delta, Vietnam. *Mangroves and Salt Marshes* 1(2) 127-135.
- [30] M. LUHAR, H.M. NEPF (2016) Wave-Induced Dynamics of Flexible Blades. *Journal of Fluids and Structures* 61 20-41.
- [31] J.L. GARZON, M. MAZA, C.M. FERREIRA, J.L. LARA, I.J. LOSADA (2019) Wave Attenuation by Spartina Saltmarshes in the Chesapeake Bay under Storm Surge Conditions. *Journal of Geophysical Research: Oceans* 124(7) 5220-5243.
- [32] L. ZHU, K. HUGUENARD, D.W. FREDRIKSSON, J. LEI (2022) Wave Attenuation by Flexible Vegetation (and Suspended Kelp) with Blade Motion: Analytical Solutions. *Advances in Water Resources* 162 104148.
- [33] A. ABDOLALI, T.J. HESSER, M. ANDERSON BRYANT, A. ROLAND, A. KHALID, J. SMITH, C. FERREIRA, A. MEHRA, M.D. SIKIRIC (2022) Wave Attenuation by Vegetation: Model Implementation and Validation Study. *Frontiers in Built Environment* 8.
- [34] T.J. VAN VEELLEN, H. KARUNARATHNA, D.E. REEVE (2021) Modelling Wave Attenuation by Quasi-Flexible Coastal Vegetation. *Coastal Engineering* 164 103820.
- [35] H. LIU, H. FANG, P. LIN (2024) A Theoretical Model for Wave Attenuation by Vegetation Considering Current Effects. *Coastal Engineering* 190 104508.
- [36] I. MAGDALENA, R. LA’LANG, R. MENDOZA (2021) Quantification of Wave Attenuation in Mangroves in Manila Bay Using Nonlinear Shallow Water Equations. *Results in Applied Mathematics* 12 100191.
- [37] I. MAGDALENA, N. KARIMA, P. DELFINA, V. FERREN (2022) Wave Damping by Breakwater and Mangrove for Protecting Shoreline. *Results in Engineering* 16 100693.

- [38] J.M. MONTGOMERY, K.R. BRYAN, J.C. MULLARNEY, E.M. HORSTMAN (2019) Attenuation of Storm Surges by Coastal Mangroves. *Geophysical Research Letters* **46**(5) 2680-2689.
- [39] Z. HU, S. LIAN, T. ZITMAN, H. WANG, Z. HE, H. WEI, L. REN, W. UJTTEWAAL, T. SUZUKI (2022) Wave Breaking Induced by Opposing Currents in Submerged Vegetation Canopies. *Water Resources Research* **58**(4) e2021WR031121.
- [40] J. WANG, G. HE, S. DEY, H. FANG (2022) Fluid–Structure Interaction in a Flexible Vegetation Canopy in an Open Channel. *Journal of Fluid Mechanics* **951** A41.
- [41] J. EL RAHI, I. MARTÍNEZ-ESTÉVEZ, B. TAGLIAFIERRO, J.M. DOMÍNGUEZ, A.J.C. CRESPO, V. STRATIGAKI, T. SUZUKI, P. TROCH (2023) Numerical Investigation of Wave-Induced Flexible Vegetation Dynamics in 3D Using a Coupling between Dual-SPHysics and the FEA Module of Project Chrono. *Ocean Engineering* **285** 115227.